

Hybrid Nanofluid Heat and Mass Transfer Characteristics Over a Stretching/Shrinking Sheet with Slip Effects

P. Sudarsana Reddy^{1,*}, P. Sreedevi¹, and Ali J. Chamkha²

¹Department of Mathematics, Rajeev Gandhi Memorial College of Engineering & Technology, Nandyal 518501, Andhra Pradesh, India

²Faculty of Engineering, Kuwait College of Science and Technology, Doha District, 35004, Kuwait

Unsteady magneto-hydrodynamic heat and mass transfer analysis of hybrid nanofluid flow over stretching/shrinking surface with chemical reaction, suction, slip effects and thermal radiation is analyzed in this problem. Combination of Alumina (Al_2O_3) and Titanium Oxide (TiO_2) nanoparticles are taken as hybrid nanoparticles and base fluid is taken as water. Using similarity transformation method the governing equations are changed in to set of ordinary differential equations. These resultant equations are numerically evaluated by utilizing Finite element method. The influence of several pertinent parameters on fluids temperature, concentration and velocity is calculated and the outcomes are plotted through graphs. The values of non-dimensional rates of heat transfer, mass transfer and velocity are also analyzed and the outcomes are represented in tables. Temperature sketches of hybrid nanofluid intensified in both unsteady and steady cases as volume fraction of both nanoparticles rises.

IP: 5.10.31.210 On: Tue, 03 Jan 2023 10:39:15

KEYWORDS: $\text{TiO}_2/\text{Al}_2\text{O}_3$ -Water Hybrid Nanofluid, Magneto-Hydrodynamics, Chemical Reaction, Slip Effects, Thermal Radiation, FEM.

1. INTRODUCTION

In recent years the idea of nanofluids has turned into more widespread area for the research people due to its gigantic range of significances in double windowpane, heat exchangers, food, biomedicine, transportation, cooling of electronic devices, etc. To intensify the common liquids thermal conductivity such as engine oils, kerosene, water, ethylene glycol, we have to suspend various varieties of nanoparticles, like, carbon nanotubes, Graphene, copper, silica, gold, silver, alumina, etc. into the common liquids. Several number of research articles are recognized in the literature which deals the augmentation of the base fluids thermal conductivity by suspending different types of nanoparticles.¹⁻⁶ Sheremet et al.⁷ deliberated heat transport analysis of single-phase model of nanofluid flow over square inclined cavity packed with water-alumina based nanofluid with the left wall is maintained sinusoidal wall temperature. Bondarenko et al.⁸ perceived cooling of heat generating and heat conducting element over an enclosure filled with water- Al_2O_3 nanofluid with moving top

wall and detected that the heated element cools down rapidly with high values of Reynolds number. Dogonchi et al.⁹ detected augmentation in the heat transfer coefficient with growing values of volume fraction of nanoparticle parameter in their work on heat transport analysis through cold external circular cylinder and hot internal rectangular cylinder filled with water-Cu based nanofluid. Bondarenko et al.¹⁰ deliberated the sway of cold vertical walls on cooling of heat generating and heat conducting source over an enclosure filled with water- Al_2O_3 based nanofluid and perceived intensification in the cooling process as nanoparticle volume fraction values rises. Mahian et al.¹¹ perceived an analysis on heat transfer analysis of single-phase, multi-phase and 3D simulation of nanofluid flows over different geometries. Mikhailenko et al.¹² professed liquid and heat transport analysis of water- Al_2O_3 based nanofluid over rotating cavities and detected worsening in the rates of heat transfer with rising values of added nanoparticle volume fraction parameter. Hashim et al.¹³ presented Finite element analysis method to find the numerical solution of nanofluid heat and flow characteristics inside a wavy cavity filled with Al_2O_3 based nanoparticles.

“Hybrid nanofluids” are special kind of fluids having better thermal conductivity compared to the nanofluids

*Author to whom correspondence should be addressed.
Email: suda1983@gmail.com
Received: 12 July 2021
Accepted: 30 June 2022

and base fluids. Hybrid nanofluids have similar kind of applications as compared with the nanofluids. The superior thermal efficiency is predicted in hybrid nanofluids because of its better performance. Hybrid nanofluids are generated by dispersing two different types of nanoparticles in the common fluid. Ahmadi et al.¹⁴ deliberated flow and heat transfer characteristics of Bungiorno's model nanofluid flow over a heated stretching surface and identified amplification in the values of Nusselt number with rising values of Brownian motion parameter. Qasim et al.¹⁵ perceived heat and mass transfer analysis of Bungiorno's model nanofluid thin film flow over a stretching sheet and noticed reduction in the values of heat transfer rates as Brownian motion parameter values rises. Biglarian et al.¹⁶ premeditated the influence of various types of nanoparticles and volume fraction of nanoparticles on heat transport and flow of unsteady nanofluid between parallel plates. Mahdy et al.¹⁷ noticed that elevation in the values of skin friction coefficient with rising values of Weissenberg number in their analysis on time-dependent hyperbolic tangential nanofluid flow over stretching wedge. Hashim et al.¹⁸ professed the influence of thermophoresis and Brownian motion on mass and heat transport features of Williamson nanofluid flow over a wedge. Astanina et al.¹⁹ deliberated unsteady natural convection flow analysis of nanofluid flow inside a partly porous cavity utilizing the thermal non-equilibrium model with heat generating solid element. Yarmand et al.²⁰ examined intensification in the heat transfer of hybrid nanofluid made up of platinum/graphene nanoplatelet–water at a four sided microchannel whose boundaries are maintained with constant heat flux. The heat transfer capabilities of Cu–Al₂O₃/water hybrid nanofluid are numerically investigated by Refs. [21, 22]. Sundar et al.²³ demonstrates the review of hybrid nanofluids and more effective heat transfer fluid characteristics of different hybrid nanofluid. Ghalambaz et al.²⁴ pioneered research on melting of nanoparticles-enhanced phase-change materials flow of hybrid nanofluid over a square cavity by using Finite element method. The impact of hybrid nanoparticles on the melting process of a nano-enhanced phase-change material in a square cavity was investigated by Ghalambaz et al.²⁵ Wei et al.²⁶ perceived the thermal conductivity enhancement of diathermic oil–SiC/TiO₂ based hybrid nanofluid flow and detected maximum of 8.39% augmentation in thermal conductivity as the concentration of suspended nanoparticle is 1 vol%. Humnic and Humnic²⁷ deliberated the heat transport analysis of two different types of hybrid nanofluids, such as, Fe₃O₄/MWCNT–water and ND/Fe₃O₄–water based nanofluid flow over tube and identified more thermal conductivity intensification in Fe₃O₄/MWCNT–water than the ND/Fe₃O₄–water hybrid nanofluid. Ghalambaz et al.²⁸ studied the flow characteristics of hybrid nanofluid inside a square porous cavity packed with MgO and Ag nanoparticles and noticed deterioration in

the values of rates of heat transfer as nanoparticle volume fraction values rises. Asadi et al.²⁹ studied thermal oil–MWCNT/Al₂O₃ hybrid nanofluid heat transfer efficiency as a cooling fluid in energy management and thermal applications. Kumar and Sarkar³⁰ theoretically and experimentally investigated heat transport enhancement of MWCNT/Al₂O₃–water nanofluid flow over minichannel heat sink and noticed intensification in the coefficient of heat transfer in the range of 30–35% as the hydraulic diameter of the decreases. Khodadadi et al.³¹ presented a review analysis on rheological properties of hybrid and mono nanofluids and perceived intensification in the fluids viscosity as nanoparticle volume fraction values rises. Sundar et al.³² experimentally examined the heat transport behavior of water–Ni/ND based hybrid nanofluid flow through a tube by considering and without considering longitudinal strip inserts and detected an augmentation of 35.43% in the rates of heat transfer values as the values of nanoparticle volume is 0.3% and Reynolds number is 22000. Hussien et al.³³ examined the heat transport features of GNPs/MWCNTs–water hybrid nanofluid flow through a mini tube and detected 43.4% augmentation in the values of Nusselt number of hybrid nanofluid. Sheikholeslami et al.³⁴ numerically analyzed the flow characteristics of MHD hybrid nanofluid arranged by captivating Fe₃O₄ and MWCNT as nanoparticles and water as base fluid inside an enclosure with double heaters and perceived intensification in the heat transfer rates. The heat transport augmentation of Fe₃O₄/MWCNT–water hybrid nanofluid inside T-shaped cavity with two porous layers and finite element technique is used to find numerical solution of the resultant equations.^{35,36} Chamkha et al.³⁷ perceived finite element technique to calculate the value of rates of heat transfer of hybrid nanofluid made by considering copper and alumina as nanoparticles and water as base fluid. Recently, Veera Krishna^{38–43} perceived the impact of hall and ion slip effects on heat transfer characteristics of nanofluid over different geometries.

Careful observation on available literature reveals that no studies have reported to investigate the sway of slip effects and chemical reaction on mass and heat transport characteristics of magneto-hydrodynamic hybrid nanofluids prepared by considering TiO₂/Al₂O₃ as nanoparticles and water as base fluid over stretching sheet. The resultant equations are solved using Finite element method with Mathematica 10.0. The problem addressed in this analysis has immediate applications in generator cooling, transformer cooling, electronic cooling etc.

2. MATHEMATICAL ANALYSIS OF THE PROBLEM

Consider unsteady, laminar, two dimensional, MHD boundary layer heat and mass transfer of TiO₂/Al₂O₃–Water based hybrid nanofluid flow through a stretching sheet with slip effects as depicted in Figure 1. Along the

stretching surface and in the direction of flow the x -axis considered and y -axis is measured normal to it. $U_w(x, t)$ is the velocity of the stretching sheet. A constant magnetic field of strength B_0 is applied normal to the plate. T_w and C_w are considered as sheet surface uniform temperature and concentration, furthermore, T_∞ and C_∞ are taken as ambient fluid temperature and concentration, correspondingly. The thermo-physical properties of the nanofluid are given in Table I. Under the above assumptions, the governing equations describing the momentum, energy and concentration in the presence of chemical reaction, slip effects and thermal radiation are given by [Asadi et al.²⁹].

$$\frac{\partial u}{\partial x} + \frac{\partial v}{\partial y} = 0 \tag{1}$$

$$\frac{\partial u}{\partial t} + u \frac{\partial u}{\partial x} + v \frac{\partial u}{\partial y} = -\frac{1}{\rho_{hnf}} \frac{\partial p}{\partial x} + \nu_{hnf} \frac{\partial^2 u}{\partial y^2} - \frac{\sigma B^2(t)}{\rho_{hnf}} u \tag{2}$$

$$\frac{\partial T}{\partial t} + u \frac{\partial T}{\partial x} + v \frac{\partial T}{\partial y} = \frac{k_{hnf}}{(\rho C_p)_{hnf}} \frac{\partial^2 T}{\partial y^2} - \frac{1}{(\rho C_p)_{nf}} \frac{\partial q_r}{\partial y} \tag{3}$$

$$\frac{\partial C}{\partial t} + u \frac{\partial C}{\partial x} + v \frac{\partial C}{\partial y} = D_B \frac{\partial^2 C}{\partial y^2} - C_1 (C - C_\infty) \tag{4}$$

The following physical boundary conditions are

$$\begin{aligned} u &= \lambda U_w = \lambda \frac{bx}{1-ct}, \quad v = v_w, \quad T = T_w + k_1 \frac{\partial T}{\partial y}, \\ C &= C_w + k_2 \frac{\partial C}{\partial y}, \quad \text{at } y = 0 \end{aligned} \tag{5}$$

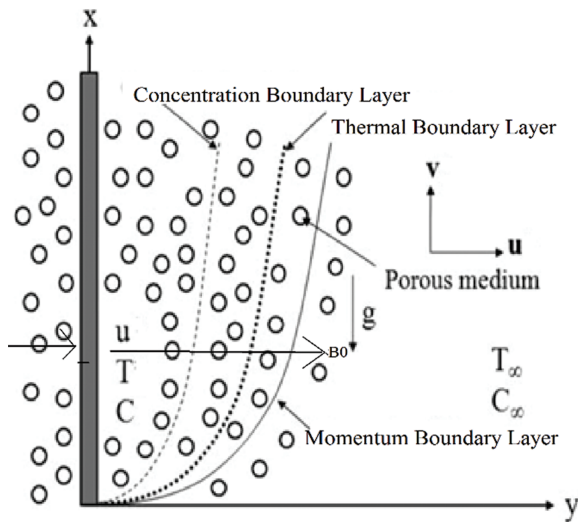


Fig. 1. Physical model and Coordinate system.

Table I. Thermo-physical properties of water and nanoparticles.

Fluid	$\rho \left(\frac{\text{Kg}}{\text{m}^3} \right)$	$C_p \left(\frac{\text{J}}{\text{kgK}} \right)$	$k \left(\frac{\text{W}}{\text{mK}} \right)$
Pure water	997.1	4179	0.613
MWCNTs	1600	796	3000
Silver (Ag)	10500	235	429

$$u \rightarrow 0, T \rightarrow T_\infty, C \rightarrow C_\infty \quad \text{at } y \rightarrow \infty \tag{6}$$

where b is positive constant, $\lambda > 0$ (stretching constant) and $\lambda < 0$ (shrinking constant).

We now presented similarity variables as

$$\begin{aligned} \eta &= y \sqrt{\frac{a}{\nu_f(1-ct)}}, \quad \psi = x \sqrt{\frac{a\nu_f}{1-ct}} f(\eta), \\ \theta(\eta) &= \frac{T - T_\infty}{T_w - T_\infty}, \quad S(\eta) = \frac{C - C_\infty}{C_w - C_\infty} \end{aligned} \tag{7}$$

Additionally,

$$\begin{aligned} U_w(x, t) &= \frac{bx}{1-ct}, \quad T_w(x, t) = T_\infty + \frac{T_0 U_w x}{\nu(1-ct)^{(1/2)}}, \\ C_w(x, t) &= C_\infty + \frac{C_0 U_w x}{\nu(1-ct)^{(1/2)}}, \quad B(t) = \frac{B_0}{(1-ct)^{(1/2)}} \end{aligned} \tag{8}$$

By utilizing Rosseland estimation for radiation, the radiative heat flux q_r is demarcated as

$$q_r = -\frac{4\sigma^*}{3K^*} \frac{\partial T^4}{\partial y} = -\frac{16\sigma^* T_\infty^3}{3K^*} \frac{\partial T}{\partial y} \tag{9}$$

The transformed equations are

$$f''' + \frac{A_2}{A_1} f f'' - \frac{A_2}{A_1} (f')^2 - \frac{A_2}{A_1} \alpha \left\{ f' + \frac{\eta}{2} f'' \right\} - A_1 M f' = 0 \tag{10}$$

$$(1 + A_4 R) \theta'' - Pr \frac{A_3}{A_4} \frac{\alpha}{2} (\eta \theta' + 2\theta') = 0 \tag{11}$$

$$S'' - Sc \frac{\alpha}{2} (\eta S' + 2S') - C_r Sc S = 0 \tag{12}$$

The associated converted boundary conditions are

$$f(0) = V_0, f'(0) = \lambda, \theta(0) = 1 + \xi \theta', S(0) = 1 + \beta S' \tag{13}$$

$$f'(\infty) \rightarrow 1, \theta(\infty) \rightarrow 0, S(\infty) \rightarrow 0 \tag{14}$$

The associated non-dimensional parameters are defined as

$$Pr = \frac{\nu_f}{\alpha_f}, \quad \alpha = \frac{c}{a}, \quad \lambda = L \left(\frac{a}{2\nu} \right), \quad M = \frac{\sigma B_0^2}{\rho a},$$

$$\xi = k_1 \left(\frac{a}{2\nu} \right),$$

$$\beta = k_2 \left(\frac{a}{2\nu} \right), \quad Sc = \frac{\nu}{D_B}, \quad C_r = \frac{C_1}{a}, \quad R = \frac{16T_\infty^3 \sigma^*}{3k^* k_f},$$

$$A_1 = \frac{1}{(1 - (\phi_1 + \phi_2))^{2.5}},$$

$$A_2 = \left[1 - (\phi_1 + \phi_2) \right] + \phi_1 \left(\frac{\rho_{s1}}{\rho_f} \right) + \phi_2 \left(\frac{\rho_{s2}}{\rho_f} \right),$$

$$A_3 = \left[1 - (\phi_1 + \phi_2) \right] + \phi_1 \left(\frac{(\rho c_p)_{s1}}{(\rho c_p)_f} \right) + \phi_2 \left(\frac{(\rho c_p)_{s2}}{(\rho c_p)_f} \right),$$

$$A_4 = \frac{k_{hnf}}{k_f}$$

The density ρ_{hnf} , thermal conductivity k_{hnf} , dynamic viscosity μ_{hnf} , and heat capacitance $(\rho c_p)_{\text{hnf}}$ of the hybrid nanoliquid are quantified by:

$$\mu_{\text{hnf}} = \frac{\mu_f}{(1 - (\phi_1 + \phi_2))^{2.5}},$$

$$\rho_{\text{hnf}} = [1 - (\phi_1 + \phi_2)] \rho_f + \phi_1 \rho_{s1} + \phi_2 \rho_{s2},$$

$$(\rho c_p)_{\text{hnf}} = [1 - (\phi_1 + \phi_2)] (\rho c_p)_f + \phi_1 (\rho c_p)_{s1} + \phi_2 (\rho c_p)_{s2},$$

$$k_{\text{hnf}} = k_{nf} * \left(\frac{k_{s2} + 2k_{nf} - 2\phi_2 (k_{nf} - k_{s2})}{k_{s2} + 2k_{nf} + \phi_2 (k_{nf} - k_{s2})} \right),$$

where

$$k_{nf} = k_f * \left(\frac{k_{s1} + 2k_f - 2\phi_1 (k_f - k_{s1})}{k_{s1} + 2k_f + \phi_1 (k_f - k_{s1})} \right)$$

The another object of this problem is to calculate skin-friction coefficient (C_f), Nusselt number (Nu_x) and Sherwood number (Sh_x) and are given as

$$C_{fx} = \frac{\tau_w}{\rho U_w^2}, \quad Nu_x = \frac{xq_w}{k_f (T_w - T_\infty)},$$

$$Sh_x = \frac{xq_m}{D_B (C_w - C_\infty)} \tag{15}$$

Where,

$$\tau_w = \mu_{\text{hnf}} \left(\frac{\partial u}{\partial y} \right)_{y=0}, \quad q_w = -k_{\text{hnf}} \left. \frac{\partial T}{\partial y} \right|_{y=0}$$

$$q_m = -D_B \left. \frac{\partial C}{\partial y} \right|_{y=0} \tag{16}$$

Using the similarity variables the above equations take the form

$$Re^{1/2} C_{fx} = \frac{1}{(1 - (\phi_1 + \phi_2))^{2.5}} f''(0),$$

$$Re^{-1/2} Nu_x = -(1 + R) A_4 \theta'(0), \quad Re^{1/2} Sh_x = -S'(0) \tag{17}$$

Where, ($Re = ((xU_w)/\nu_f)$) represents the local Reynolds number.

3. NUMERICAL SOLUTION OF THE PROBLEM

The variational Finite element process⁴⁵ is applied to estimate numerically aforementioned Eqs. (10)–(12) with boundary conditions (13) and (14). Compare to other numerical methods finite element method is the better method to solve both ordinary and partial differential equations numerically.

4. RESULTS AND DISCUSSION

The impact of slip effects on heat transport coefficient of TiO₂/Al₂O₃–Water hybrid nanoliquid flow over stretching

sheet is analyzed in this analysis. Variations in the sketches of concentration, temperature and velocity with respect to influenced parameters are calculated and plotted through graphs from Figures 2–22. Comparison of present numerical code with existing values is made and depicted in Table II.

Figures 2–7 reflect the sway of volume fraction of parameters ϕ_1 and ϕ_2 on the concentration, temperature and velocity sketches for both stretching and shrinking cases of TiO₂/Al₂O₃–Water hybrid nanoliquid. The velocity scatterings depreciate with escalating values of both ϕ_1 and ϕ_2 for stretching case, however, scatterings of

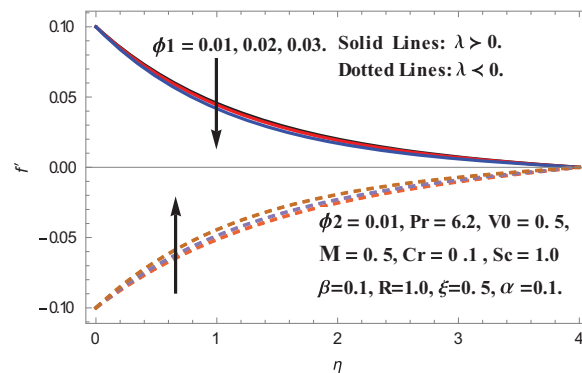


Fig. 2. The Effect of (ϕ_1) on f' .

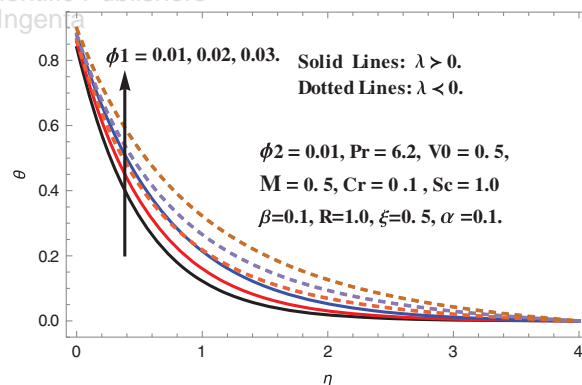


Fig. 3. The Effect of (ϕ_1) on θ .

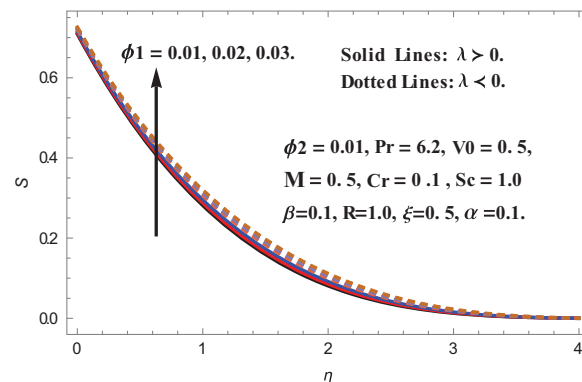


Fig. 4. The Effect of (ϕ_1) on S .

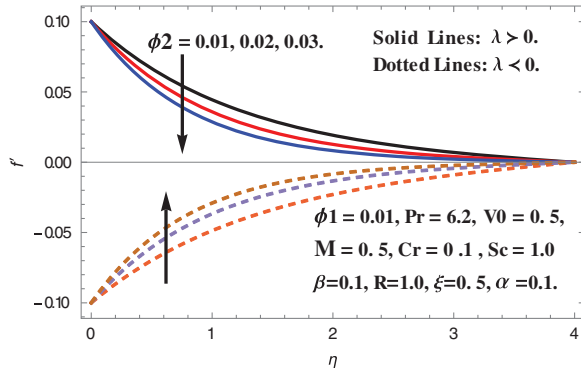


Fig. 5. The Effect of (ϕ_2) on f' .

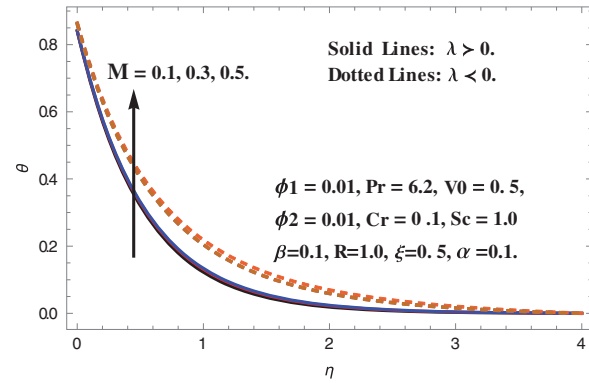


Fig. 9. The Effect of (M) on θ .

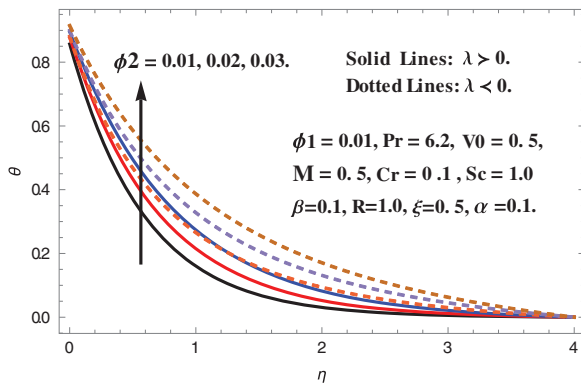


Fig. 6. The Effect of (ϕ_2) on θ .

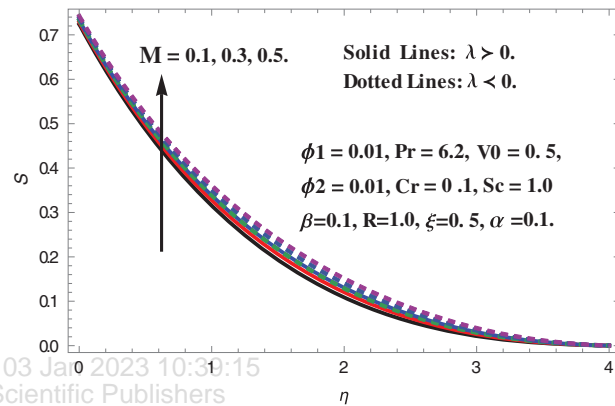


Fig. 10. The Effect of (M) on S .

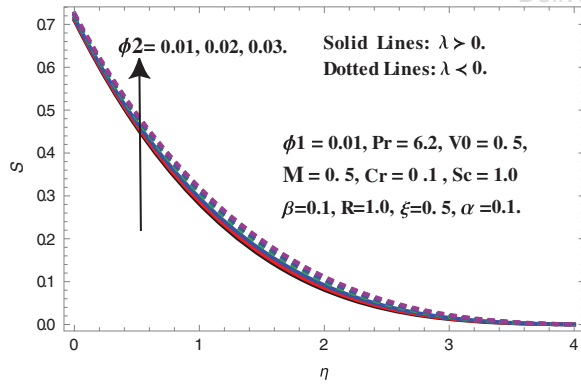


Fig. 7. The Effect of (ϕ_2) on S .

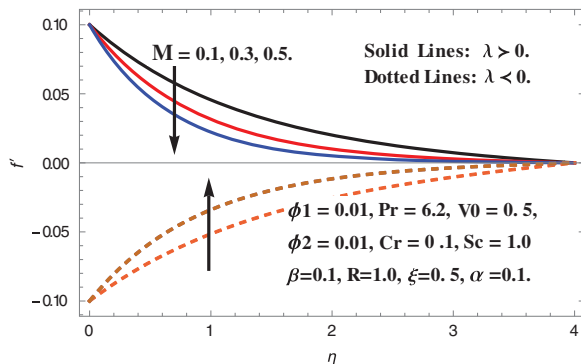


Fig. 8. The Effect of (M) on f' .

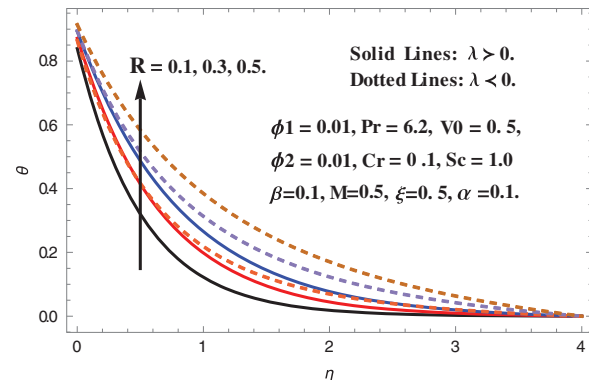


Fig. 11. The Effect of (R) on θ .

IP: 5.10.31.210 On: Tue, 03 Jan 2023 10:30:15
 Copyright: American Scientific Publishers
 Delivered by Ingenta

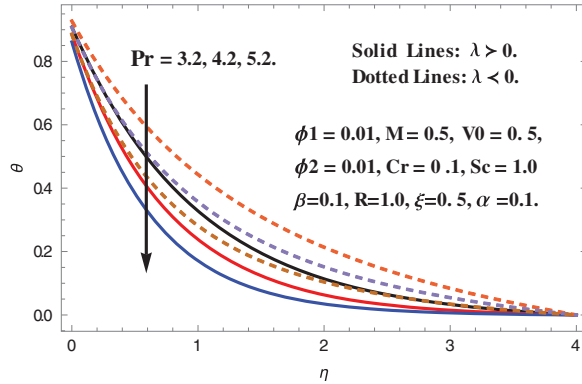


Fig. 12. The Effect of (Pr) on θ .

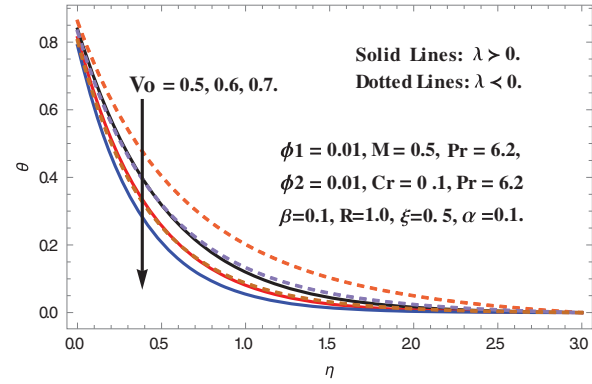


Fig. 16. The Effect of (V_0) on θ .

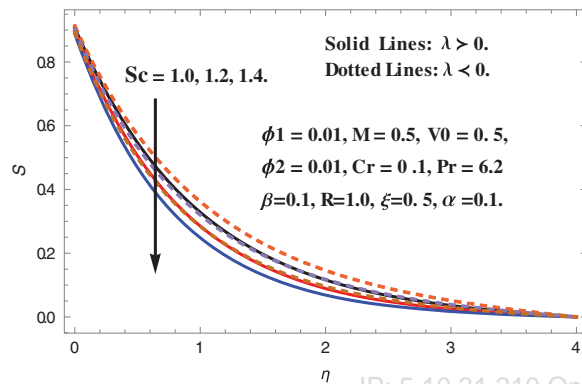


Fig. 13. The Effect of (Sc) on S .

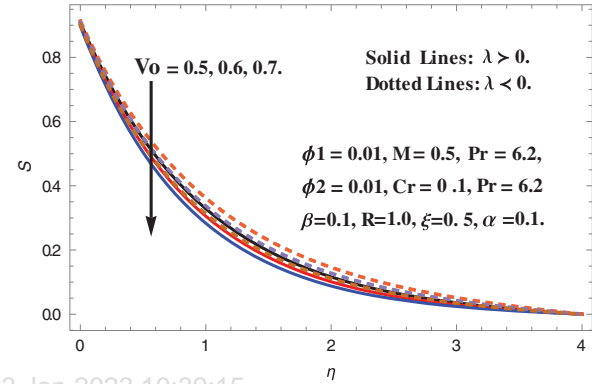


Fig. 17. The Effect of (V_0) on S .

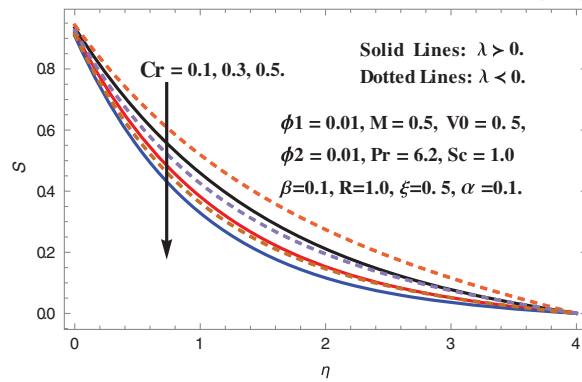


Fig. 14. The Effect of (Cr) on S .

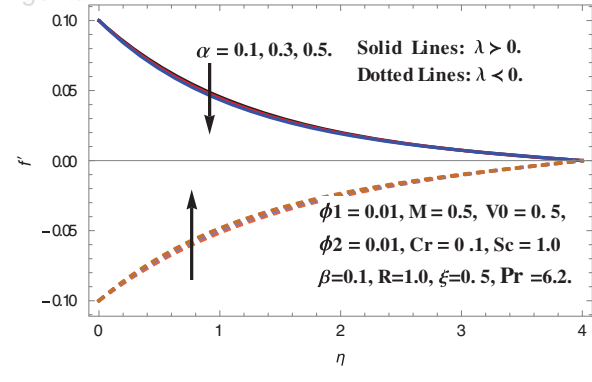


Fig. 18. The Effect of (α) on f' .

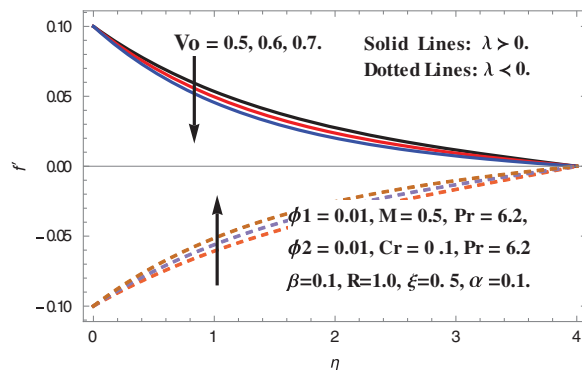


Fig. 15. The Effect of (V_0) on f' .

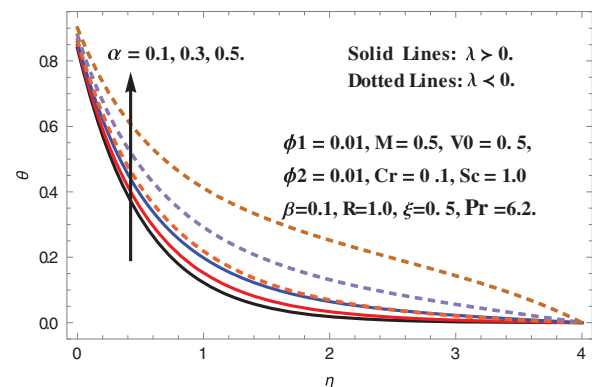


Fig. 19. The Effect of (α) on θ .

IP: 5.10.31.210 On: Tue, 03 Jan 2023 10:39:15
 Copyright: American Society of Mechanical Engineers
 Delivered by Ingenta

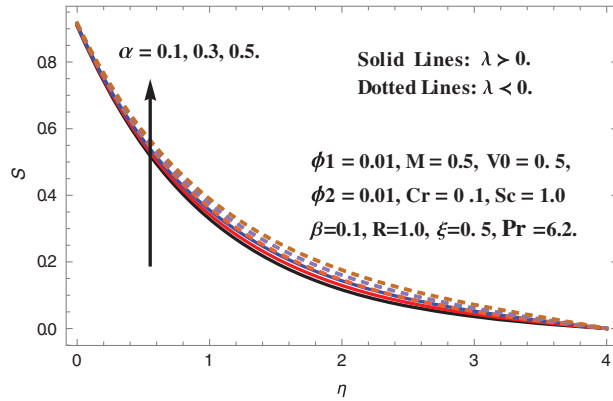


Fig. 20. The Effect of (α) on S .

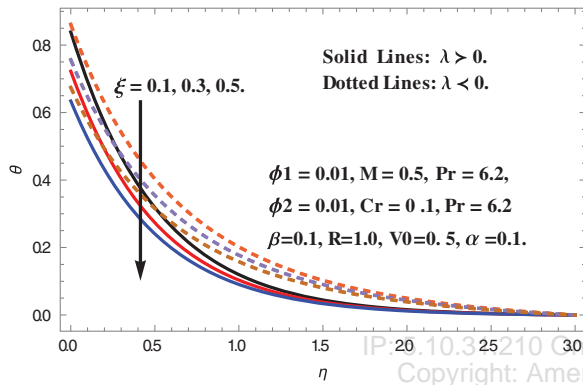


Fig. 21. The Effect of (ξ) on θ .

velocity intensifies in shrinking cases of $\text{TiO}_2/\text{Al}_2\text{O}_3$ -Water hybrid nanofluid with escalating values of (M). The scatterings of temperature and concentration in both stretching and shrinking cases of $\text{TiO}_2/\text{Al}_2\text{O}_3$ -Water hybrid nanofluid with respect to Magnetic parameter (M) are depicted in Figures 9 and 10. The concentration and temperature scattering optimizes with magnifying values of (M) and this amplifying nature is reasonably lesser in stretching case than shrinking case of $\text{TiO}_2/\text{Al}_2\text{O}_3$ -Water hybrid nanofluid.

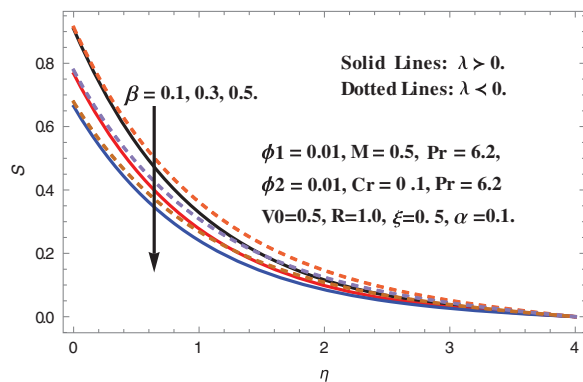


Fig. 22. The Effect of (β) on S .

Thermal boundary layer thickness with altered values of Radiation parameter (R) in both stretching and shrinking cases of $\text{TiO}_2/\text{Al}_2\text{O}_3$ -Water hybrid nanofluid are portrayed in Figure 11. Thermal boundary layer thickness upsurges with cumulating values of (R) in both stretching and shrinking cases of $\text{TiO}_2/\text{Al}_2\text{O}_3$ -Water hybrid nanofluid. Furthermore, this cumulating tendency is marginally more in shrinking case than stretching case of $\text{TiO}_2/\text{Al}_2\text{O}_3$ -Water hybrid nanofluid. Figure 12 exemplifies the disparities in sketches of temperature with altered values of Prandtl number (Pr) in both stretching and shrinking cases of $\text{TiO}_2/\text{Al}_2\text{O}_3$ -Water hybrid nanofluid. The temperature sketches worsen with up surging values of (Pr) and this phenomenon is marginally higher in stretching case than shrinking case of $\text{TiO}_2/\text{Al}_2\text{O}_3$ -Water hybrid nanofluid.

$\text{TiO}_2/\text{Al}_2\text{O}_3$ -Water based hybrid nanofluid concentration shrinks in both shrinking and stretching cases with improving values of (Sc). Additionally, the depreciating nature in concentration sketches is more in stretching case than shrinking case of $\text{TiO}_2/\text{Al}_2\text{O}_3$ -Water based hybrid nanofluid (Fig. 13). Figure 14 exhibits significance of chemical reaction parameter (Cr) on concentration depicts in both stretching and shrinking cases of $\text{TiO}_2/\text{Al}_2\text{O}_3$ -Water based Hybrid nanofluid. The concentration sketches deteriorate with cumulated values of (Cr) in both stretching and shrinking cases.

Figures 15–17 professed the disparities in the thickness of hydrodynamic, thermal boundary layer and solutal boundary layers with altered values of suction parameter (V_0) in both stretching and shrinking cases of $\text{TiO}_2/\text{Al}_2\text{O}_3$ -Water based hybrid nanofluid. The thickness of hydrodynamic boundary layer escalates with amplifying values of (V_0) in stretching case, nevertheless, it deteriorates in shrinking case and is shown in Figure 15. The thickness of thermal and solutal boundary layers diminished with step up values of (V_0) as depicted in Figures 16 and 17. Furthermore, the escalating nature in the thickness of hydrodynamic boundary layer and diminishing nature in the thickness of thermal boundary layer and solutal boundary layers is slightly more stretching case than shrinking case of $\text{TiO}_2/\text{Al}_2\text{O}_3$ -Water based hybrid nanofluid.

The impact of unsteadiness parameter (α) on scatterings of concentration, temperature and velocity is depicted in

Table II. Comparison of $(-\theta'(0))$ with the results of Waini et al.⁴⁴ for various values of (Pr) and $\phi_1 = 0, \phi_2 = 0$.

Parameter	Waini et al. ⁴⁴	Present results
Pr	$(-\theta'(0))$	$(-\theta'(0))$
2.0	0.911353	0.911341
6.13	1.759682	1.759676
7.0	1.895400	1.895397
20.0	3.353902	3.353915

Figures 18–20 and perceived that the fluids velocity diminishes in stretching case, however, it amplifies in shrinking case with improving values of (α) of $\text{TiO}_2/\text{Al}_2\text{O}_3$ –Water based hybrid nanofluid. Nevertheless, temperature and concentration sketches amplify with intensifying values of (α) in both stretching and shrinking cases of $\text{TiO}_2/\text{Al}_2\text{O}_3$ –Water based hybrid nanofluid. Furthermore, it can be seen that the amplifying nature in temperature, concentration depicts is marginally more in shrinking case than stretching case of $\text{TiO}_2/\text{Al}_2\text{O}_3$ –Water based Hybrid nanofluid.

Figure 21 describes the sway of temperature slip parameter (ξ) on thermal boundary layer thickness in both stretching and shrinking cases of $\text{TiO}_2/\text{Al}_2\text{O}_3$ –Water based hybrid nanofluid. With up surging values of (ξ) , temperature sketches degenerate in both cases and this degenerating phenomenon is slightly more in stretching case hybrid nanofluid than shrinking case of hybrid nanofluid.

The concentration sketches of $\text{TiO}_2/\text{Al}_2\text{O}_3$ –Water based hybrid nanofluid worsens in both stretching and shrinking cases as concentration slip parameter (β) codes intensifies and this nature in solutal boundary layer thickness is slightly more in stretching case than shrinking cases of $\text{TiO}_2/\text{Al}_2\text{O}_3$ –Water based hybrid nanofluid and is shown in Figure 22.

Tables III and IV reveal the sway of pertinent parameters on non-dimensional rates of mass transport, heat transfer and rates of velocity in both stretching and shrinking cases of $\text{TiO}_2/\text{Al}_2\text{O}_3$ –Water based hybrid nanofluid. It is perceived from Table III that the values of skin-friction coefficient values elevates, however, values of Nusselt number deteriorates in both stretching and shrinking cases of $\text{TiO}_2/\text{Al}_2\text{O}_3$ –Water based hybrid nanofluid as the values of ϕ_1 and ϕ_2 rises. The values of Sherwood number diminishes in stretching case, nevertheless,

Table III. Values of skin-friction coefficient $(f''(0))$, local Nusselt number $(-\theta'(0))$ and local Sherwood number $(-S'(0))$.

Parameters					$f''(0)$		$-\theta'(0)$		$-S'(0)$	
ϕ_1	ϕ_2	M	Pr	R	Stretching	Shrinking	Stretching	Shrinking	Stretching	Shrinking
0.01	0.01	0.5	6.2	1	0.24943	0.2098	4.89547	4.13461	0.91815	0.86944
0.02	0.01	0.5	6.2	1	0.25767	0.22792	4.35542	3.62642	0.9179	0.87005
0.03	0.01	0.5	6.2	1	0.27804	0.25773	3.75483	3.09508	0.91729	0.87101
0.01	0.01	0.5	6.2	1	0.80216	0.70956	9.99249	8.31996	0.9179	0.87005
0.01	0.02	0.5	6.2	1	1.01649	0.99296	4.02366	3.41384	0.91595	0.87279
0.01	0.03	0.5	6.2	1	1.2361	1.22399	3.09239	2.76032	0.91425	0.87463
0.01	0.01	0.1	6.2	1	0.13307	0.11193	2.85661	2.41264	0.91815	0.86944
0.01	0.01	0.3	6.2	1	0.197	0.18434	2.8353	2.46132	0.91492	0.87344
0.01	0.01	0.5	3.2	1	0.25649	0.19854	2.81873	2.48523	0.91257	0.88745
0.01	0.01	0.5	4.2	1	0.13307	0.11193	1.62333	1.2967	0.91815	0.86944
0.01	0.01	0.5	5.2	1	0.1325	0.11195	2.04909	1.65503	0.91814	0.85958
0.01	0.01	0.5	6.2	1	0.13125	0.11254	2.45214	2.03138	0.91745	0.84575
0.01	0.01	0.5	6.2	0.1	0.13307	0.11193	2.35661	2.41264	0.91815	0.86944
0.01	0.01	0.5	6.2	0.3	0.13325	0.11195	2.33557	1.86546	0.91802	0.86954
0.01	0.01	0.5	6.2	0.5	0.13354	0.11198	1.9079	1.5327	0.90254	0.87565

Table IV. Values of skin-friction coefficient $(f''(0))$, local Nusselt number $(-\theta'(0))$ and local Sherwood number $(-S'(0))$.

Parameters					$f''(0)$		$-\theta'(0)$		$-S'(0)$	
Cr	V_0	α	ξ	β	Stretching	Shrinking	Stretching	Shrinking	Stretching	Shrinking
0.1	0.5	0.1	0.5	0.1	0.13307	0.11193	2.85663	2.41264	0.64825	0.57001
0.3	0.5	0.1	0.5	0.1	0.13304	0.11168	2.85642	2.41254	0.79963	0.74023
0.5	0.5	0.1	0.5	0.1	0.13225	0.11145	2.85632	2.41023	0.91815	0.86944
0.1	0.5	0.1	0.5	0.1	0.10543	0.0835	0.87768	0.25077	0.7367	0.67101
0.1	0.6	0.1	0.5	0.1	0.11858	0.0969	1.87744	1.16666	0.8129	0.76522
0.1	0.7	0.1	0.5	0.1	0.13307	0.13293	2.85663	2.43264	0.92815	0.86944
0.1	0.5	0.1	0.5	0.1	0.13327	0.11193	2.85661	2.41264	0.91815	0.86944
0.1	0.5	0.3	0.5	0.1	0.13944	0.11966	2.7181	2.15112	0.90009	0.8519
0.1	0.5	0.5	0.5	0.1	0.1456	0.12702	2.53208	1.75757	0.88185	0.83432
0.1	0.5	0.1	0.1	0.1	0.13307	0.11193	2.86434	2.46374	0.91815	0.86944
0.1	0.5	0.1	0.3	0.1	0.13215	0.11235	2.46677	2.16376	0.91804	0.87012
0.1	0.5	0.1	0.5	0.1	0.13205	0.11345	2.16612	1.92893	0.77577	0.87562
0.1	0.5	0.1	0.5	0.1	0.13307	0.11193	2.86493	2.46378	0.91815	0.36944
0.1	0.5	0.1	0.5	0.3	0.13202	0.11075	2.84522	2.26253	0.77577	0.79065
0.1	0.5	0.1	0.5	0.5	0.13025	0.11042	2.83225	2.25122	0.67152	0.84509

values of Sherwood number intensifies in shrinking case of $\text{TiO}_2/\text{Al}_2\text{O}_3$ -Water based hybrid nanofluid as the values of ϕ_1 and ϕ_2 rises. The non-dimensional values of (C_f) and (Sh_x) rises in both stretching and shrinking cases with (M) intensifies. Furthermore, (Nu_x) values deteriorates in stretching case, however, they intensifies in shrinking case with (M) . The values of skin friction coefficient degenerates in stretching case, whereas, elevate in shrinking case as (Pr) values rises. With rise in the values of (Pr) , the dimensionless values of (Nu_x) are hiked, however, (Sh_x) values deteriorates in both stretching and shrinking cases. As the values of (R) improves the values of non-dimensional skin friction coefficient amplifies, whereas, values of Nusselt number worsens in both stretching and shrinking cases of $\text{TiO}_2/\text{Al}_2\text{O}_3$ -Water based hybrid nanofluid. The values of Sherwood number degenerates in stretching case, however, intensifies in shrinking case with (R) . It is clear from Table IV that the values of (C_f) and (Nu_x) deteriorates in both stretching and shrinking cases of hybrid nanofluid as the values of (Cr) intensifies. The influence of (Cr) on rates of mass transfer coefficient is also perceived in Table IV and found elevation in (Sh_x) values. The non-dimensional rates of velocity, mass and heat transfer values optimizes in both cases of hybrid nanofluid as the values of (V_0) upsurges. As the values of (α) rises the values $(f''(0))$ amplifies, whereas, the values $(-\theta'(0))$ and $(-S'(0))$ worsens in both stretching and shrinking cases of $\text{TiO}_2/\text{Al}_2\text{O}_3$ -Water based hybrid nanofluid. The non-dimensional rates of velocity and mass transfer values deteriorates in stretching case, however, elevates in shrinking case with improved values of (ξ) . However, with higher value of (ξ) the values of (Nu_x) diminishes in both stretching and shrinking cases. Finally, in both stretching and shrinking cases the values of (C_f) and (Nu_x) depreciates with amplifying values of (β) . Furthermore, (Sh_x) values degenerates in stretching case, however, upgrades in shrinking case as (β) values optimizes.

5. CONCLUSION

The present study has addressed $\text{TiO}_2/\text{Al}_2\text{O}_3$ -Water based hybrid nanofluid heat and mass transfer analysis over a stretching/shrinking sheet. The impact of velocity slip, temperature slip, chemical reaction and thermal radiation on $\text{TiO}_2/\text{Al}_2\text{O}_3$ -Water based hybrid nanofluid flow is also analyzed. The most noteworthy findings are as follows:

- (i) Volume fraction parameters of both nanofluids ϕ_1 and ϕ_2 intensifies the temperature of $\text{TiO}_2/\text{Al}_2\text{O}_3$ -Water based hybrid nanofluid in both stretching and shrinking cases.
- (ii) Suction parameter (V_0) deteriorates the temperature and concentration of $\text{TiO}_2/\text{Al}_2\text{O}_3$ -Water based hybrid nanofluid in both stretching and shrinking cases.
- (iii) Both temperature and concentration sketches amplify with rising values of unsteadiness parameter (α) in both

stretching and shrinking cases of $\text{TiO}_2/\text{Al}_2\text{O}_3$ -Water based hybrid nanofluid.

(iv) Rising values of (M) leads amplification in the values of Sherwood number and skin-friction coefficient.

(v) The dimensionless rates of heat transfer shrinks with rising values of (ξ) in both stretching and shrinking cases of $\text{TiO}_2/\text{Al}_2\text{O}_3$ -Water based hybrid nanofluid.

NOMENCLATURE

C_f	Skin-friction coefficient
ϕ_2	Nanoparticle volume fraction of Silver
k_f	Thermal conductivity of basefluid
Nu_x	Nusselt number
ϕ_1	Nanoparticle volume fraction of MWCNT
Re_x	Local Reynolds number
C_∞	Ambient fluid concentration
u_∞	Velocity of mainstream
T_w	Wall constant temperature
T_∞	Ambient temperature
T	Fluid temperature
C	Fluid concentration
q_w	Wall heat flux
J_w	Wall mass flux
f	Dimensionless stream function
u_w	Velocity of the wall
K^*	Mean absorption coefficient
σ^*	Stephan-Boltzmann constant
Sh_x	Sherwood number
Pr	Prandtl number
(u, v)	Velocity components in x- and y-axis
R	Radiation parameter
τ_w	Shear stress
Sc	Schmidt number
M	Magnetic field parameter
D_m	Diffusion coefficient
Sc	Schmidt number
U	Composite velocity
(x, y)	Direction along and perpendicular to the wedge
C_r	Chemical reaction parameter
V_0	Suction parameter
C_w	Concentration at the wall
$s1$	First solid component
$s2$	Second solid component

Greek Symbols

α	Thermal diffusivity of base fluid
ν	Kinematic viscosity
μ	Fluid viscosity
ρ_p	Nanoparticle mass density
S	Dimensionless nanoparticle volume fraction
η	Similarity variable
θ	Dimensionless temperature
λ	Velocity slip parameter
σ	Electrical conductivity
ξ	Thermal slip parameter

Subscripts

- ∞ Condition far away from cone surface
- Hnf* hybrid nanofluid
- f* Base fluid
- nf* Nanofluid

Superscripts

- ' Differentiation with respect to η

References and Notes

1. S. U. S. Choi, Z. G. Zhang, W. Yu, F. E. Lockwood, and E. A. Grulke, *Appl. Phys.* 79, 2252 (2001).
2. J. A. Eastman, S. U. S. Choi, S. Li, W. Yu, and L. J. Thompson, *Appl. Phys.* 78, 718 (2001).
3. M. Ghalambaz, A. Behseresht, J. Behseresht, and A. J. Chamkha, *Advanced Powder Technology* 26, 224 (2015).
4. R. Ellahi, M. Hassan, and A. Zeeshan, *Asia-Pac. J. Chem. Eng.* 11, 179 (2016).
5. P. Sudarsana Reddy and A. J. Chamkha, *Adv. Powder Technol.* 27, 1207 (2016).
6. P. Sudarsana Reddy and P. Sreedevi, *The European Physical Journal Plus* 136, 1 (2021).
7. M. A. Sheremet, I. Pop, and A. V. Rosca, *International Journal of Numerical Methods for Heat and Fluid Flow* 28, 1738 (2018).
8. D. S. Bondarenko, M. A. Sheremet, H. F. Oztop, and M. E. Ali, *J. Therm. Anal. Calorim.* 136, 673 (2018).
9. A. S. Dogonchi, M. A. Sheremet, D. D. Ganji, and I. Pop, *J. Therm. Anal. Calorim.* 135, 1171 (2018).
10. D. S. Bondarenko, M. A. Sheremet, H. F. Oztop, and M. E. Ali, *Int. J. Heat Mass Transfer* 130, 564 (2019).
11. O. Mahian, L. Kolsi, Mohammad Amani, P. Estellé, G. Ahmadi, C. Kleinstreuer, J. S. Marshall, M. Siavashi, R. A. Taylor, H. Niazmand, S. Wongwises, T. Hayat, A. Kolanjiyil, A. Kasaeian, and I. Pop, *Physics Reports* 790, 1 (2019).
12. S. A. Mikhailenko, M. A. Sheremet, H. F. Oztop, and N. Abu-Hamdeh, *International Journal of Mechanical Sciences* 156, 137 (2019).
13. I. Hashim, A. I. Alsabery, M. A. Sheremet, and A. J. Chamkha, *Adv. Powder Technol.* 30, 399 (2019).
14. A. R. Ahmadi, A. Zahmatkesh, M. Hatami, and D. D. Ganji, *Powder Technol.* 258, 125 (2014).
15. M. Qasim, Z. H. Khan, R. J. Lopez, and W. A. Khan, *The European Physical Journal Plus* 131, 1 (2016).
16. M. Biglarian, M. Rahimi Gorji, O. Pourmehran, and G. Domairry, *Int. J. Hydrogen Energy* 42, 22005 (2017).
17. A. Mahdy and A. J. Chamkha, *International Journal of Numerical Methods for Heat and Fluid Flow* 28, 2567 (2018).
18. Hashim, M. Khan, and A. Hamid, *Int. J. Heat Mass Transfer* 118, 480 (2018).
19. M. S. Astanina, M. Sheremet, and C. J. Umavathi, *International Journal of Numerical Methods for Heat and Fluid Flow* 29, 1902 (2019).
20. H. Yarmand, S. Gharekhani, G. Ahmadi, S. F. S. Shirazi, S. Baradaran, E. Montazer, M. N. M. Zubir, M. S. Alehashem, S. N. Kazi, and M. Dahari, *Energy Convers. Manage.* 100, 419 (2015).
21. M. R. A. Rahman, K. Y. Leong, A. C. Idris, M. R. Saad, and M. Anwar, *Heat Mass Transfer* 53, 1835 (2016).
22. S. A. M. Mehryan, F. M. Kashkooli, M. Ghalambaz, and A. J. Chamkha, *Adv. Powder Technol.* 28, 2295 (2017).
23. L. S. Sundar, K. V. Sharma, M. K. Singh, and A. C. M. Sousa, *Renewable and Sustainable Energy Reviews* 68, 185 (2017).
24. M. Ghalambaz, A. Doostani, A. J. Chamkha, and M. A. Ismael, *International Journal of Mechanical Sciences* 134, 85 (2017).
25. M. Ghalambaz, A. Doostani, E. Izadpanahi, and A. J. Chamkha, *Journal of the Taiwan Institute of Chemical Engineers* 72, 104 (2017).
26. B. Wei, C. Zou, X. Yuan, and X. Li, *Int. J. Heat Mass Transfer* 107, 281 (2017).
27. G. Huminic and A. Huminic, *Int. J. Heat Mass Transfer* 119, 813 (2018).
28. M. Ghalambaz, M. A. Sheremet, S. A. M. Mehryan, F. M. Kashkooli, and I. Pop, *J. Therm. Anal. Calorim.* 135, 1381 (2018).
29. A. Asadi, M. Asadi, A. Rezaniakolaei, L. A. Rosendahl, M. Afrand, and S. Wongwises, *Int. J. Heat Mass Transfer* 117, 474 (2018).
30. V. Kumar and J. Sarkar, *International Communications in Heat and Mass Transfer* 91, 239 (2018).
31. H. Khodadadi, S. Aghakhani, H. Majd, R. Kalbasi, S. Wongwises, and M. Afrand, *Int. J. Heat Mass Transfer* 127, 997 (2018).
32. L. S. Sundar, M. K. Singh, and A. C. M. Sousa, *Int. J. Heat Mass Transfer* 121, 390 (2018).
33. A. A. Hussien, M. Z. Abdullah, N. M. Yusop, W. Al-Kouz, E. Mahmoudi, and M. Mehrali, *Entropy* 21, 480 (2019).
34. M. Sheikholeslami, S. A. M. Mehryan, A. Shafee, and M. A. Sheremet, *J. Mol. Liq.* 277, 388 (2019).
35. M. Izadi, H. F. Oztop, M. A. Sheremet, S. A. M. Mehryan, and N. Abu-Hamdeh, *Numerical Heat Transfer, Part A: Applications* 76, 479 (2019).
36. S. A. M. Mehryan, M. A. Sheremet, M. Soltani, and M. Izadi, *J. Mol. Liq.* 277, 959 (2019).
37. A. J. Chamkha, S. Sazegar, E. Jamesahar, and M. Ghalambaz, *Energies* 12, 541 (2019).
38. M. Veera Krishna, *Heat Transfer* 49, 1920 (2020).
39. M. Veera Krishna, *Heat Transfer* 49, 2311 (2020).
40. M. Veera Krishna, *Heat Transfer* 49, 1374 (2020).
41. M. Veera Krishna, *International Communications in Heat and Mass Transfer* 119, 104927 (2020).
42. M. Veera Krishna, *Chin. J. Chem. Eng.* 34, 40 (2021).
43. M. Veera Krishna and G. S. Reddy, *The Journal of Analysis* 27, 103 (2018).
44. I. Waini, A. Ishak, and I. Pop, *Int. J. Heat Mass Transfer* 136, 288 (2019).
45. P. Sudarsan Reddy and D. R. V. Prasada Rao, *Journal of Applied Fluid Mechanics* 5, 139 (2012).